Earth and Planetary Science Letters 468 (2017) 27–37

Contents lists available at ScienceDirect

Earth and Planetary Science Letters

www.elsevier.com/locate/epsl

New insights into cycling of ^{231}Pa and ^{230}Th in the Atlantic Ocean ☆

Johannes Rempfer [a,b,*], Thomas F. Stocker [a,b], Fortunat Joos [a,b], Jörg Lippold [c,b], Samuel L. Jaccard [c,b]

[a] Climate and Environmental Physics, Physics Institute, University of Bern, Sidlerstrasse 5, 3012 Bern, Switzerland
[b] Oeschger Centre for Climate Change Research, University of Bern, 3012 Bern, Switzerland
[c] Institute of Geological Sciences, University of Bern, Baltzerstrasse 1+3, 3012 Bern, Switzerland

ARTICLE INFO

Article history:
Received 4 December 2015
Received in revised form 7 March 2017
Accepted 23 March 2017
Available online xxxx
Editor: H. Stoll

Keywords:
^{231}Pa
^{230}Th
boundary scavenging
bottom scavenging
reversible scavenging
AMOC-strength

ABSTRACT

We use the Bern3D model of intermediate complexity to examine the marine cycle of isotopes ^{231}Pa and ^{230}Th and the relationship between the particle-bound ratio Pa_p/Th_p and changes in the formation of the North Atlantic Deep Water (NADW). Model parameters describing reversible scavenging of isotopes by organic particles, opal, calcite and resuspended sediments were systematically varied and alternative sink parametrisations explored. It proves difficult to simultaneously achieve a good agreement with observations of dissolved and particle-associated concentrations of ^{231}Pa and ^{230}Th (Pa_d, Th_d, Pa_p, Th_p) as well as the particle-bound ratio Pa_p/Th_p within the classical concept of reversible scavenging alone.
Agreement between simulated and observed Pa_d, Th_d and estimates of mean ocean residence times is improved by taking into account simplified representations of additional sinks at the sea floor (bottom scavenging) and at continental boundaries (boundary scavenging). We also find improved agreement between model and data by increasing lateral advection, in particular for Pa_d. These results point to the importance of sink processes that act in addition to reversible scavenging to shape the steady state distribution of ^{231}Pa and, to a lesser degree, of ^{230}Th.
In transient experiments in which the strength of the Atlantic meridional overturning circulation (AMOC) is periodically turned on and off, we find a strong statistical relationship between variations in AMOC strength and Pa_p/Th_p at great depths in the Northwest Atlantic region. These conclusions are robust across the range of sink parametrisations, that are consistent with estimates in the mean ocean residence time of ^{231}Pa and ^{230}Th. Our results indicate that the relationship between Pa_p/Th_p and AMOC-strength may not be fundamentally affected by uncertainties in sink processes, at least on the large spatial and temporal scale considered here, and support the idea that changes in Pa_p/Th_p in sediments of the Northwest Atlantic are indicative of changes in AMOC strength. Taking into account our simplified approach, our results indicate that the relationship between Pa_p/Th_p and AMOC-strength in the deep Northwest Atlantic is not affected by boundary scavenging or bottom scavenging. Our results thus support the idea that changes in Pa_p/Th_p in sediments of the Northwest Atlantic are indicative of changes in AMOC strength.

1. Introduction

The purpose of this study is to improve the understanding of the cycling of ^{230}Th and ^{231}Pa in the Atlantic Ocean. We present results from sensitivity experiments with our model where we apply idealised representations of sediment resuspensions by bottom currents (nepheloid layers) and preferential removal of radionuclides at continental margins (boundary scavenging), as well as a stronger AMOC. Agreement between observed and simulated profiles of dissolved (Pa_d, Th_d) and particle-bound (Pa_p, Th_p) activities as well as of the dissolved and particle-bound ^{231}Pa to ^{230}Th ratios ($^{231}Pa_d/^{230}Th_d$, $^{231}Pa_p/^{230}Th_p$) in the Atlantic, is evaluated by statistical means (Taylor, 2001). Furthermore, we examine the relationship between Pa_p/Th_p and AMOC-strength in transient experiments where AMOC is periodically turned on and off. As a considerable progress over previous studies, the coupling of a biogeochemical model allows us to consistently simulate effects of changes in the export of biogenic particles, in response to changes in ocean circulation and the nutrient balance of the surface ocean (e.g., Plattner et al., 2001; Schmittner, 2005).

Due to the long residence time of uranium in seawater (>100 kyr), radionuclides ^{231}Pa ($t_{1/2} = 32.5$ kyr) and ^{230}Th ($t_{1/2} =$

☆ Marine cycling of ^{231}Pa and ^{230}Th.

* Corresponding author.
E-mail address: rempfer@climate.unibe.ch (J. Rempfer).

http://dx.doi.org/10.1016/j.epsl.2017.03.027

75.2 kyr) are uniformly produced within the water column by decay of ^{235}U and ^{234}U, respectively. ^{231}Pa and ^{230}Th are subject to adsorption to and desorption from particle surfaces and are readily removed from the water column by settling particles (reversible scavenging) (Bacon and Anderson, 1982). As ^{230}Th is strongly particle reactive, its residence time in seawater, τ_{Th}, is only a few decades. Th_d almost linearly increases with depth due to the process of reversible scavenging. ^{231}Pa is relatively less particle reactive and has a longer residence time ($\tau_{Pa} \approx 100$–200 yr) (Bacon and Anderson, 1982; Anderson et al., 1983b; Yu et al., 1996; Moran et al., 2002). Depth profiles of Pa_d deviate from linearity, and show little increase below depths of 1–2 km (Moran et al., 2002). Such depth evolution cannot be explained by reversible scavenging alone (Nozaki and Nakanishi, 1985) and has been associated with various processes of lateral mixing towards regions of high particle flux (boundary scavenging) (Anderson et al., 1983a; Moran et al., 2002; Roy-Barman, 2009; Christl et al., 2010), bottom scavenging by resuspended sediments, i.e., nepheloid layers (Deng et al., 2014; Hayes et al., 2015b), and lateral export by water masses (Luo et al., 2010).

The ratio of particulate ^{231}Pa and particulate ^{230}Th (Pa_p/Th_p thereafter) has been proposed to reflect the rate of the meridional overturning circulation (MOC) (Yu et al., 1996; McManus et al., 2004; Gherardi et al., 2009).

An important characteristic of the cycling of ^{231}Pa and ^{230}Th is their differential affinity to sinking particles, resulting in preferential scavenging of ^{230}Th relative to ^{231}Pa (Walter et al., 1997; Chase et al., 2002; Kretschmer et al., 2011). The different affinity of ^{231}Pa and ^{230}Th to particle type i is reflected by the so-called fractionation factor, $f_i(\mathrm{Th/Pa})$ (Anderson et al., 1983b; Henderson et al., 1999)

$$f_i(\mathrm{Th/Pa}) = \frac{(\mathrm{Th/Pa})_{p,i}}{(\mathrm{Th/Pa})_d} = \frac{K_i^{\mathrm{Th}}}{K_i^{\mathrm{Pa}}} = f_i, \tag{1}$$

where $K_i^j = A_{p,i}^j \cdot \rho/(A_d^j \cdot C_i)$, with A_d^j dissolved activity of isotope j, ρ density of seawater, $A_{p,i}^j$ particle-bound activity, and C_i concentration of particle type i. Substantial variations of fractionation factors with latitude and depth from about 1–40 have been observed which mainly reflect the variable composition of particle export (Walter et al., 1997; Moran et al., 2002; Scholten et al., 2005; Hayes et al., 2015b).

A number of studies using models of different complexity, have been performed to gain better understanding of the marine cycle of Pa and Th (Siddall et al., 2005; Dutay et al., 2009; Roy-Barman, 2009) and the effect of AMOC-strength on the distribution of Pa_p/Th_p at the seafloor (Marchal et al., 2000; Siddall et al., 2007; Luo et al., 2010). Some of these models rely on a simplified approach in terms of model geometry or ocean dynamics (Marchal et al., 2000; Luo et al., 2010), or they lack a dynamic coupling of biogenic particle fluxes to circulation and nutrient availability (Siddall et al., 2005, 2007). Moreover, some models suffer from weaknesses in the realistic simulation of Th_d, and in particular Pa_d (Siddall et al., 2005; Dutay et al., 2009).

2. Methods

We use the Bern3D ocean model of intermediate complexity (Müller et al., 2006), coupled to an energy-moisture balance model (Ritz et al., 2011). The resolution of the ocean model is 36 × 36 grid cells in the horizontal, equidistant in longitude and in the sine of latitude. Spacing of the 32 depth layers is logarithmic, increasing with depth from 39 m at the surface to 397 m in the deepest layer. The ocean model contains a biogeochemical module which calculates export production of biogenic particles such as calcite ($CaCO_3$), opal, and particulate organic carbon (POC) from prognostic equations (Fig. A1). Annual export production from the euphotic zone is comparable to available estimates (Tschumi et al., 2008; Rempfer et al., 2011). Biological productivity (i.e., production of POC) in the euphotic zone (uppermost 75 m) is controlled by temperature, light, phosphate and iron and follows the parametrisation of Doney et al. (2006) (Tschumi et al. (2008), Parekh et al. (2008)). Remineralisation and redissolution of POC, opal and $CaCO_3$ in the water column below 75 m takes place instantaneously and follows prescribed profiles (e.g. based on Martin, 1990) as outlined in Rempfer et al. (2011, their equations 2, 3a, 3b).

^{231}Pa and ^{230}Th are included into the Bern3D model following Bacon and Anderson (1982), Marchal et al. (2000) and Siddall et al. (2005). For the calculation of adsorption constants we follow two different approaches: For the 2d-approach (Marchal et al., 2000) we assume no remineralisation and redissolution of biogenic particles with depth. For the 3d-approach (Siddall et al., 2005) we take into account remineralisation and redissolution of POC, opal and calcite below the euphotic zone (see section 3 for details on the experimental set-up). We assume the 3d-approach to be more realistic as it includes differential particle dissolution and remineralisation. Besides, it is consistent with the simulation of Nd isotopes within the Bern3D model (Rempfer et al., 2011).

The main source of ^{231}Pa and ^{230}Th in the ocean is radioactive ingrowth from uranium decay, which is homogeneously distributed throughout the ocean. Sinks of ^{231}Pa and ^{230}Th are radioactive decay and removal from the water column by settling particles. ^{231}Pa and ^{230}Th are adsorbed onto particle surfaces and are released back to the water column by remineralisation and dissolution of particles at depth. The physical process of adsorption onto and desorption from particle surfaces is called reversible scavenging and is known to play an important role in the marine cycle of a number of isotopes (Bacon and Anderson, 1982; Marchal et al., 2000; Siddall et al., 2005; Oka et al., 2009; Rempfer et al., 2011).

The conservation equations of dissolved and particle-bound ^{231}Pa and ^{230}Th activities are:

$$\frac{\delta A_d^j}{\delta t} = \mathbf{T}(A_d^j) + \beta^j + k_{-1}^j \cdot A_p^j - (k_1^j + \lambda^j) \cdot A_d^j \tag{2}$$

$$\frac{\delta A_p^j}{\delta t} = \mathbf{T}(A_p^j) - \frac{\delta(w_s \cdot A_p^j)}{\delta z} - (k_{-1}^j + \lambda^j) \cdot A_p^j + k_1^j \cdot A_d^j, \tag{3}$$

where A_d^j corresponds to the dissolved activity ($\mathrm{dpm\,m^{-3}\,yr^{-1}}$) and A_p^j to the particle-bound activity ($\mathrm{dpm\,m^{-3}\,yr^{-1}}$) of isotopes ^{231}Pa and ^{230}Th, as denoted by the index j (see Table 1 for a list of symbols, abbreviations and values). $\mathbf{T}$ is the transport operator accounting for advection, diffusion and convection, as simulated by the Bern3D model (Müller et al., 2006). k_{-1}^j denotes the uniform desorption constants taken as 2.4 $\mathrm{yr^{-1}}$ for both isotopes, k_1^j denotes adsorption constants ($\mathrm{yr^{-1}}$), β^j is the production of ^{231}Pa and ^{230}Th from U-decay ($\mathrm{dpm\,m^{-3}\,yr^{-1}}$), λ^j is the constant for radioactive decay ($\mathrm{yr^{-1}}$), and w_s is the particle settling velocity taken as globally uniform (1000 $\mathrm{m\,yr^{-1}}$).

Adsorption rate constants are calculated for every grid cell and each isotope j:

$$k_1^j(\theta, \phi, z) = \sum_{i=1}^{M} \sigma_i^j \cdot F_i(\theta, \phi, z). \tag{4}$$

where F_i denotes the flux ($\mathrm{mol\,m^{-2}\,yr^{-1}}$) of particle type i (POC, opal, $CaCO_3$, resuspended lithogenic material – litho) for the given grid cell at longitude (θ), latitude (ϕ) and depth (z). σ_i^j defines the scavenging efficiency ($\mathrm{m^2\,mol^{-1}}$) for each particle type i for ^{231}Pa

Table 1
List of symbols, abbreviations and values.

Symbol	Variable	Value	Units
j	Index for ^{231}Pa, ^{230}Th		
A_d^j	Dissolved activity		$dpm\,m^{-3}\,yr^{-1}$
A_p^j	Particle-associated activity		$dpm\,m^{-3}\,yr^{-1}$
i	Index for particle type		
F_i	Particle flux		$mol\,m^{-2}\,yr^{-1}$
v	Globally uniform settling velocity	1000	$m\,yr^{-1}$
β^{Pa}	Production of ^{231}Pa from U-decay	$2.33 \cdot 10^{-3}$	$dpm\,m^{-3}\,yr^{-1}$
β^{Th}	Production of ^{230}Th from U-decay	$2.52 \cdot 10^{-2}$	$dpm\,m^{-3}\,yr^{-1}$
λ^{Pa}	Decay constant ^{231}Pa	$2.13 \cdot 10^{-5}$	yr^{-1}
λ^{Th}	Decay constant ^{230}Th	$9.22 \cdot 10^{-6}$	yr^{-1}
k_{-1}^j	Desorption constant ^{231}Pa, ^{230}Th	2.4	yr^{-1}
k_1^j	Adsorption constant ^{231}Pa, ^{230}Th	Eq. (4)	yr^{-1}
f_i	Fractionation factor, particle type i	Table A1	
$g_{ca,op}^{Pa}$	Relative affinity factor, ^{231}Pa on $CaCO_3$, opal	Table A1	
σ_0	Reference scavenging efficiency	Table A1	$m^2\,mol^{-1}$
σ_i^j	Scavenging efficiency of i by particle type j	Eq. (5c)–(6a)	$m^2\,mol^{-1}$

and ^{230}Th. The relationship between flux F_i and concentration M_i is given by $M_i = \frac{J_i * F_i}{w_s}$, where J_i is the molar mass (g mol^{-1}).

Following Marchal et al. (2000) values of scavenging efficiency σ_i^j, which are required for the calculation of adsorption constants (equation (4)), are defined as indicated in equations (5a)–(6b). These particle-specific adsorption constants, are derived from a reference scavenging efficiency, σ_0 ($m^2\,mol^{-1}$), and are used for model tuning (Tables A1, A2), viz.,

$$\sigma_{POC}^{Pa} = \sigma_0 \cdot f_{POC} \tag{5a}$$

$$\sigma_{ca}^{Pa} = \sigma_0 \cdot f_{ca} \tag{5b}$$

$$\sigma_{op}^{Pa} = \sigma_0 \cdot f_{ca} \cdot g_{ca,op}^{Pa} = \sigma_{ca}^{Pa} \cdot g_{ca,op}^{Pa} \tag{5c}$$

$$\sigma_{litho}^{Pa} = \sigma_0 \cdot f_{litho} \tag{5d}$$

$$\sigma_{POC,ca,litho}^{Th} = \sigma_0 \cdot 1 \tag{6a}$$

$$\sigma_{op}^{Th} = \sigma_0 \cdot f_{ca} \cdot g_{ca,op}^{Pa} \cdot f_{op}^{-1} = \sigma_{op}^{Pa} \cdot f_{op}^{-1} \tag{6b}$$

Fractionation factors f_i describe the fractionation of ^{231}Pa and ^{230}Th by a certain particle type i (equation (1)), $g_{ca,op}^{Pa}$ describes the relative affinity of ^{231}Pa to opal compared to $CaCO_3$: $g_{ca,op}^{Pa} = \frac{\sigma_{ca}^{Pa}}{\sigma_{op}^{Pa}}$. We assume that ^{230}Th adsorbs equally on POC, $CaCO_3$ and litho (equation (6a)). We note that some uncertainty is associated with the exact value of desorption and adsorption rates. Our values are similar to that of previous studies by Marchal et al. (2000) and Luo et al. (2010).

Regarding the fractionation of ^{231}Pa and ^{230}Th by individual particle types we rely on observations (see Table A1 for a compilation of values). However, less information is available on the relative affinity of ^{231}Pa or ^{230}Th to different particle types (as indicated e.g., by $g_{ca,op}^{Pa}$) (Walter et al., 1997; Chase et al., 2002; Scholten et al., 2005). In modelling approaches these scaling constants are generally used as tuning parameters and it is therefore not surprising that differences emerge between studies (Marchal et al., 2000; Siddall et al., 2005; Dutay et al., 2009).

It has been suggested that bottom scavenging in nepheloid layers acts as an additional sink for ^{231}Pa and ^{230}Th at the seafloor and is shaping profiles of Pa_d and Th_d (Anderson et al., 1983b; Thomas et al., 2006; Okubo et al., 2012; Deng et al., 2014; Hayes et al., 2015b). Our model is too coarse for a dynamical simulation of processes which lead to the formation of nepheloid layers (Biscaye and Eittreim, 1977). Therefore, and consistent with recent observations (Lam et al., 2015, 40 to 1650 µg/L) we assume a globally uniform concentration of resuspended lithogenic material (litho) in grid cells which are adjacent to sediment of 60 µg/L. The thickness of the nepheloid layer depends on the thickness of the corresponding bottom grid cell which increases with depth from 39 m at the surface to 397 m in the deepest layer. Besides and in agreement with Deng et al. (2014) we assume that nepheloid layers preferentially remove ^{231}Pa relative to ^{230}Th (factor of 10).

At ocean margins Pa has been reported to be removed from the water column more efficiently than in the open ocean (Anderson et al., 1983a). In order to examine the effect of boundary scavenging of Pa in particular on Pa_d we scale export production (and thus adsorption coefficients) in grid cells at continental boundaries by a factor 2, within the module describing the cycle of Pa. Thus, this scaling does not affect the cycling of nutrients, oxygen, and carbon within the model.

We are aware that our approaches for taking into account bottom scavenging and boundary scavenging are simplifications. This is consistent with the aim of this study to present sensitivity experiments based on idealised simulations to identify the first-order processes controlling the marine cycling of ^{231}Pa and ^{230}Th.

3. Overview of experiments and evaluation of model performance

The Bern3D model is a climate model of intermediate complexity suitable for long-term paleoclimate and large ensemble studies. Parameters are tuned such that atmospheric and surface ocean temperature, sea surface salinity, sea ice cover, Atlantic and Pacific zonal mean temperature, salinity, and radiocarbon are simulated in reasonable agreement with observations (Ritz et al., 2011). Compared to other models and available estimates (13 to 23 Sv, Talley et al., 2003; Srokosz and Bryden, 2015), simulated AMOC strength (≈14 Sv) is at the lower end of the estimated range. In this study we aim to investigate processes which are important for the simulation of Pa and Th in agreement with observations. In particular regarding Pa one important process is advection (e.g., Marchal et al., 2000; Luo et al., 2010). We therefore examine an alternative steady-state where AMOC strength is increased to ≈18 Sv (Fig. A3a) by increasing the Atlantic-to-Pacific freshwater-flux (see Table A2 for further details). The AMOC strength can only be increased to a certain degree by increasing the Atlantic-to-Pacific freshwater-flux. The model becomes numerically unstable for very large freshwater fluxes.

Based on the control 3d-approach (parameter set Re3d, Table A2) we aim to improve agreement between simulated and observed values of Pa_d, Th_d, Pa_d/Th_d and Pa_p/Th_p by taking into account additional sinks (1) at the sea floor, i.e., bottom scavenging of Pa and Th in a simplified representation of nepheloid

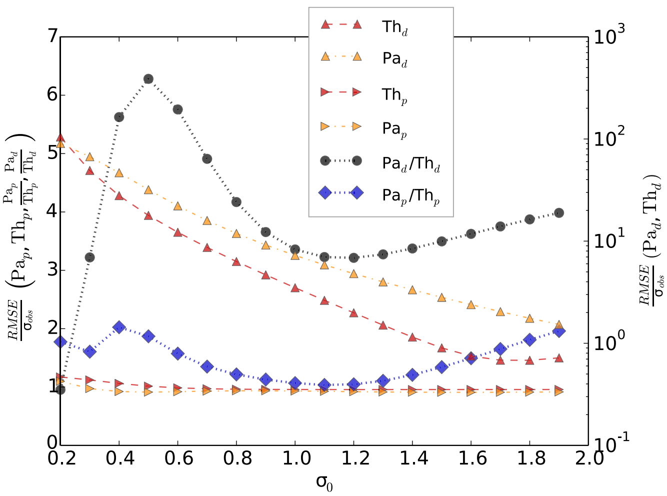

Fig. 1. Root mean squared error (RMSE) of simulated from observed values, divided by standard deviation of observed values (σ_{obs}) for Pa$_d$, Th$_d$ (right y-axis, note the log-scale), Pa$_p$, Th$_p$, Pa$_d$/Th$_d$ and Pa$_p$/Th$_p$ (left y-axis) for experiments where reference scavenging efficiency, σ_0, was increased from 0.2 to 1.9. Except for σ_0 the parameter sets equal Re3d respectively (see Table A2 for further details).

layers (Re3d_Bt) and (2) at the ocean margins, i.e., boundary scavenging of Pa in a simplified representation of increased particle flux at ocean margins (Re3d_Bd). We also consider the case (3) where bottom scavenging and boundary scavenging are combined (Re3d_BtBd) and (4) show results from a transient experiment with stronger overturning circulation (Re3d_BtBd_Fw). Finally (5), we present results from an experiment which is similar to Re3d_BtBd_Fw but which is based on the 2d-approach (Re2d_BtBd_Fw) of Marchal et al. (2000). In the second part of the study we examine the effect of changes in AMOC-strength on Pa$_p$/Th$_p$ in the Northwest Atlantic, by applying periodic freshwater perturbations (±0.3 Sv, similar to Rempfer et al., 2012) to the North Atlantic (45 to 70°N). We focus on the deep Northwest Atlantic as the discussion on the role of variations in AMOC during past climate changes has also largely focused on this region (e.g., McManus et al., 2004; Ritz et al., 2013; Böhm et al., 2015). Beyond that, Pa$_p$/Th$_p$ in the deep Northwest Atlantic was reported to be sensitive to AMOC variations (Luo et al., 2010) and the Bern3D model is able to simulate large-scale features of the AMOC (Ritz et al., 2011; Rempfer et al., 2011). We note that our experiments and analyses, aimed to investigate changes in the deep Northwest Atlantic, do not allow to conclude on the relationship between overturning circulation and Pa$_p$/Th$_p$ in other regions.

An adequate value of σ_0 is determined by minimising the deviation (i.e., the root mean squared error, $RMSE = \frac{1}{(N-1)} \times \sum_{k=1}^{N} \sqrt{(sim_k - obs_k)^2}$, divided by the standard deviation of observations σ_{obs}) between simulated (sim_k) and observed (obs_k) values of Pa$_d$, Th$_d$, Pa$_p$, Th$_p$ and Pa$_p$/Th$_p$ (k is an index over all observations N). Furthermore, agreement between observed and

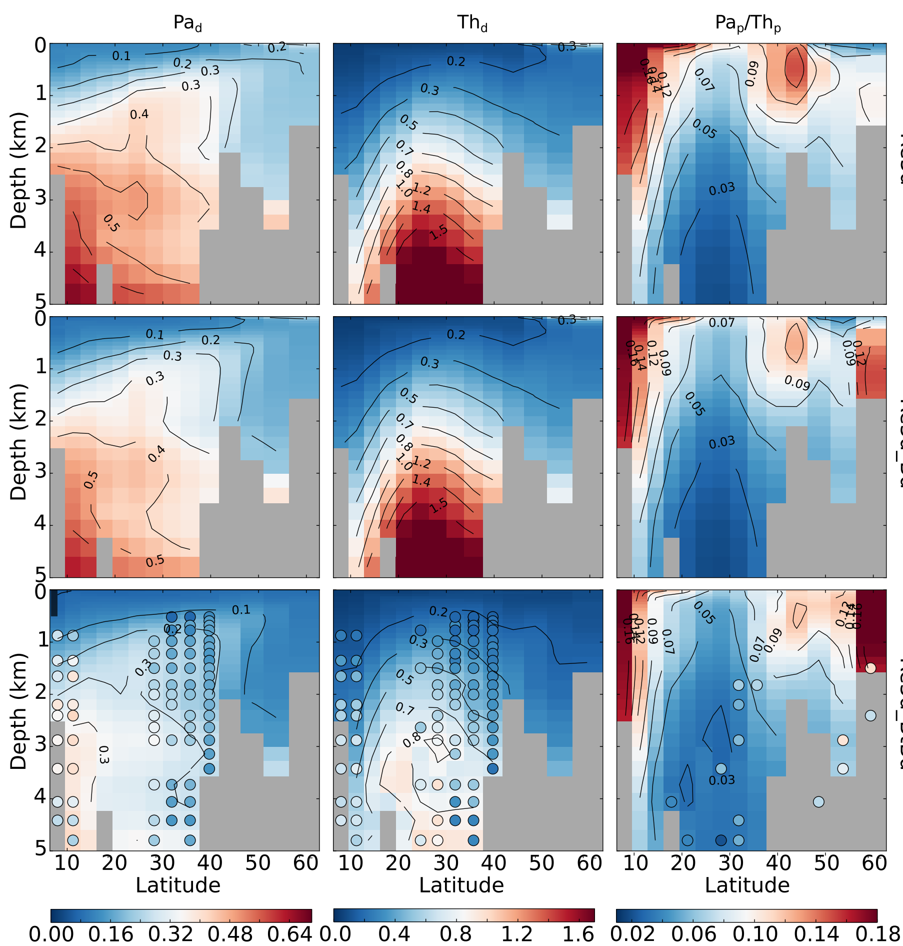

Fig. 2. Simulated Pa$_d$, Th$_d$ and Pa$_p$/Th$_p$ (indicated on top of the figure) along GEOTRACES transect GA03 (Hayes et al., 2015b) (the course of the track is indicated in Fig. A4) as obtained from experiments Re3d, Re3d_Bd, Re3d_BtBd (indicated at the right side of the figure). Available observations from the water column (Pa$_d$, Th$_d$) and sediment surfaces (Pa$_p$/Th$_p$) are superimposed using the same colorscale. (For interpretation of the references to colour in this figure legend, the reader is referred to the web version of this article.)

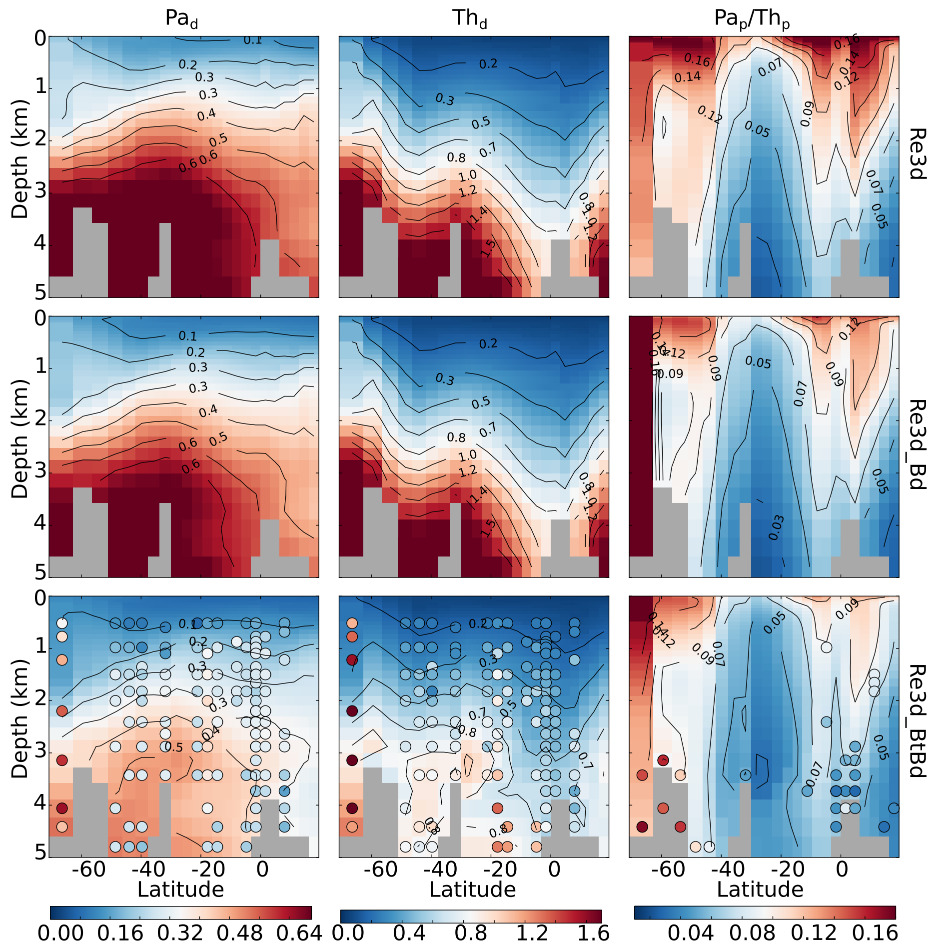

Fig. 3. Simulated Pa_d, Th_d and Pa_p/Th_p (indicated on top of the figure) along GEOTRACES transect GA02S (Deng et al., 2014) (the course of the track is indicated in Fig. A4) as obtained from experiments Re3d, Re3d_Bd, Re3d_BtBd (indicated at the right side of the figure). Available observations from the water column (Pa_d, Th_d) and sediment surfaces (Pa_p/Th_p) are superimposed using the same colorscale. (For interpretation of the references to colour in this figure legend, the reader is referred to the web version of this article.)

simulated values is evaluated by means of correlation coefficient, root mean squared error and relative standard deviation which are summarised in a Taylor-plot (Taylor, 2001).

Observational data have been compiled using data from the references listed in Table A3, yielding a stack of 537 Th_d, 111 Th_p, 360 Pa_d, 45 Pa_p and 52 core-top Pa_p/Th_p data points (the distribution of observations of Pa_d, Th_d, Pa_p/Th_p on the Bern3D model grid is indicated in Fig. A3). As no thorough intercalibration has been carried out in studies preceding the GEOTRACES project, data quality may differ between studies. The evaluation of such an effect, however, is beyond the scope of this manuscript. Therefore, and due to the relatively small number of available observations, we assume all published data to be valid. Information on particle-affinity (Walter et al., 1997; Chase et al., 2002; Kretschmer et al., 2011), fractionation factors (Walter et al., 1997; Moran et al., 2002; Hayes et al., 2015b), and residence times (Bacon and Anderson, 1982; Anderson et al., 1983b; Yu et al., 1996; Moran et al., 2002) is used for the evaluation of the different models on a qualitative basis.

4. The modern-day marine cycle of ^{231}Pa and ^{230}Th

The model value for the efficiency of reversible scavenging (σ_0, equation (4)) for model setup Re3d is determined from observations. σ_0 is varied over a large range (Fig. 1), while keeping all other parameters constant. Results are compared with observations of Pa_p, Th_p, Pa_d, Th_d and Pa_p/Th_p. For Pa_p/Th_p a distinct minimum of *RMSE* is observed around 1.0 (Fig. 1). For Th_d, Th_p, Pa_d and Pa_p *RMSE* is decreasing slowly with increasing σ_0. Hence, for the following simulations we choose $\sigma_0 = 1.0$ as it represents a reasonable compromise with regard to *RMSE* for Pa_d, Th_d and Pa_p/Th_p.

Modelled Pa_d, Th_d concentrations are substantially overestimated in the deep Atlantic when applying parameter set Re3d (Figs. 2, 3 and blue solid line in Fig. 4a, b). Similarly, variability and absolute values of Pa_d/Th_d are overestimated by the model throughout the water column (Fig. 4c). In contrast, simulated Atlantic Pa_p/Th_p is in reasonable agreement with observations (Fig. 4d). The agreement with observations is quantified in Fig. 5 (blue markers with solid border line). Unrealistically large Th_d and Pa_d values result in high global mean residence times τ_{Pa} (310 yr) and τ_{Th} (42 yr) which are at the upper end of the estimated ranges for ^{231}Pa (100–200 yr) and ^{230}Th (a few decades) (Bacon and Anderson, 1982; Anderson et al., 1983b; Yu et al., 1996; Moran et al., 2002). Note, in this manuscript residence times are obtained from steady-state as ratios of the total inventories (i.e., particulate and dissolved) and the globally integrated radioactive ingrowth of ^{231}Pa and ^{230}Th.

The effect of associated near-bottom scavenging on profiles of Pa_d and Th_d is investigated next. We apply a globally uniform concentration of resuspended particles of 60 μg/L to grid cells which are adjacent to sediment (suffix _bt in experiment label, Table A2). We assume that particle-bound Pa and Th are in equilibrium with dissolved concentrations and that the settling speed of

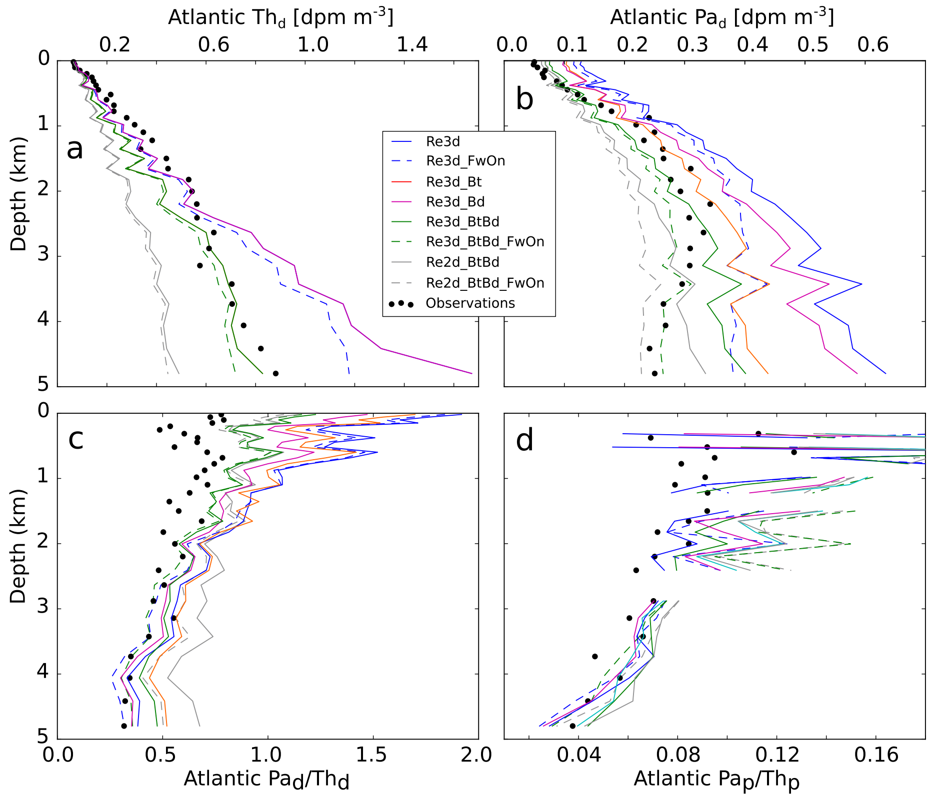

Fig. 4. Profiles of observed (indicated by black dots, see Table A3, for references) and simulated (a) Th_d (b) Pa_d, (c) Pa_d/Th_d, and (d)Pa_p/Th_p. Simulated values are taken from grid cells where observations are available. If more than one observation is available at one depth, the weighted mean is shown. Gaps in profiles of Pa_p/Th_p are due to missing observations at certain depths. Details on experiments are given on panel as well as in Table A2. The suffix FwOn indicates the on-state from experiments in which AMOC is turned on and off every 10 kyr by applying positive and negative freshwater perturbations (±0.3 Sv, similar to Rempfer et al. (2012)) to the North Atlantic surface (45 to 70°N). As boundary scavenging does not affect Th, Th_d from experiments Re3d and Re3d_Bd as well as Re3d_Bt and Re3d_BtBd are identical. (For interpretation of the references to colour in this figure legend, the reader is referred to the web version of this article.)

resuspended particles equals w_s (see Table 1). Furthermore, we assume that ^{230}Th is scavenged 10 times more efficiently than ^{231}Pa ($f_{litho} = 10$, Tables A1, A2).

Taking into account bottom scavenging in _bt improves the agreement between simulated and observed Pa_d and Th_d (Figs. 2, 3 and green solid lines, Fig. 4a, b). τ_{Pa} and τ_{Th} are reduced to 220 and 28 yr and are in better agreement with available observational estimates. Note that even stronger bottom scavenging, which may help for obtaining more realistic Pa_d, leads to stronger and unrealistic depletion of Th_d at the seafloor (not shown). From this and based on the results shown in Figs. 2, 3, and 4a, b we conclude that bottom scavenging may provide an explanation for certain characteristics in profiles of Pa_d and Th_d but that additional processes affect the vertical distributions in particular of Pa_d.

Although not well-quantified, the concept of boundary scavenging is assumed to play an important role for the removal of adsorption-prone elements with residence times greater than about 100 yr (Anderson et al., 1983a; Yu et al., 1996; Roy-Barman, 2009). The Bern3D model does not allow an explicit simulation of processes like lithogenic input and nutrient input via rivers or submarine groundwater discharge, which may lead to increased particle flux at ocean boundaries (Siddall et al., 2005). We take into account boundary scavenging by scaling particle fluxes (and thus adsorption constants) of POC, opal, $CaCO_3$ and resuspended lithogenic material (litho) in grid cells which are adjacent to continents by a factor of 2. Additional simulations were performed using scaling factors of 4 and 10 (not shown). Overall, the effect of boundary scavenging on Pa_d and Pa_p/Th_p appears less important than the effect of bottom scavenging. Note that the factor of 2 may rather be interpreted as an additional tuning factor and, again due to the coarse resolution of our model, can barely be compared to observations at specific locations. Margins were reported to be preferential sinks for Pa (Anderson et al., 1983a; Lippold et al., 2012; Hayes et al., 2015a). In our simplified approach we assume that boundary scavenging affects only Pa.

Overall, boundary scavenging leads to smaller values of Pa_d (_bd, Figs. 2, 3, and solid red line in Fig. 4b) which is also reflected in smaller τ_{Pa} (280 yr). As boundary scavenging does not affect Th in our model, Th_d and τ_{Th} of _bd are equal to Re3d (Fig. 4a).

For illustrative purposes we combine bottom scavenging and boundary scavenging in parameter set Re3d_BtBd (turquoise solid line in Fig. 4, turquoise markers with solid border line in Fig. 5), which leads to better overall agreement between observed and simulated Pa_d. Simulated τ_{Pa} and τ_{Th} (220 and 28 yr) are consistent with available observations (Bacon and Anderson, 1982; Anderson et al., 1983b; Yu et al., 1996). However, despite reasonable agreement between simulated and observed Pa_d at depths shallower than 2.5 km, simulated Pa_d exceeds observations at greater depths.

Summing up results of parameter sets Re3d_Bt, Re3d_Bd and Re3d_BtBd we find that Pa_d/Th_d and in particular Pa_p/Th_p are only slightly affected by boundary and/or bottom scavenging (solid green, red and turquoise lines in Fig. 4c, d). However, agreement between simulated and observed Pa_p/Th_p is slightly reduced for Re3d_BtBd compared to Re3d (Fig. 5). Due to the simplified representation of bottom and boundary scavenging in our approach, we prefer not to put too much emphasis on these small changes. Detailed experiments with more sophisticated models are needed in this regard.

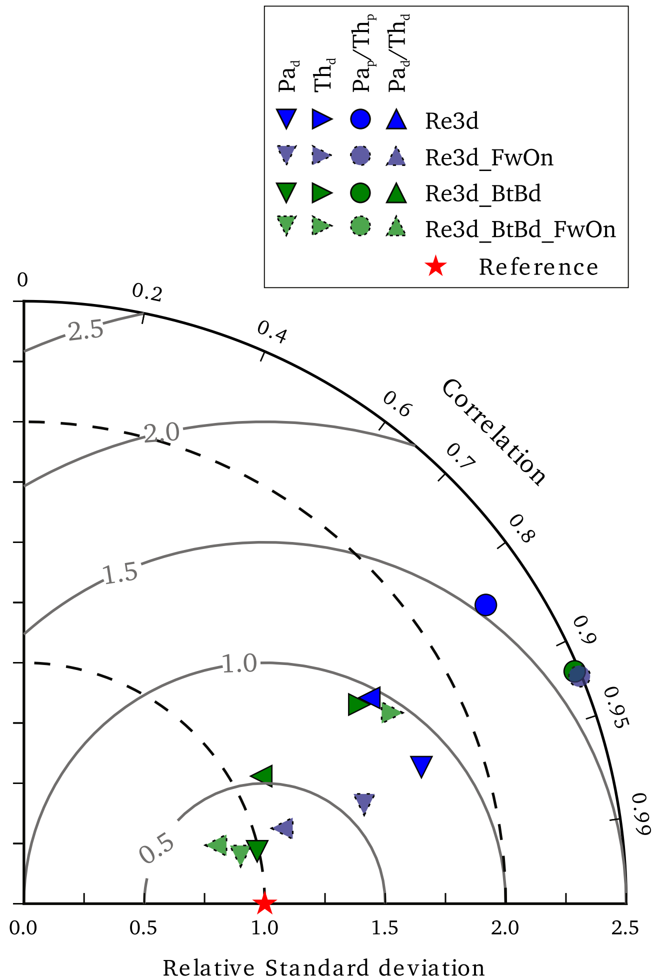

Fig. 5. Taylor diagram (Taylor, 2001) providing information about the relative standard deviation (on the x-axis), the correlation coefficients (given by the azimuthal position) and RMSE (solid grey lines on panel) between simulated and available measurements of Pa_d, Th_d, Pa_p/Th_p and Pa_d/Th_d, for parameter sets Re3d and Re3d_BtBd for two different AMOC-strengths ($\approx$ 18 and 25 Sv). Simulated values are taken from grid cells where observations are available. If more than one observation is available at one depth, the weighted mean is shown. Markers for AMOC on-states are transparent (referring to an AMOC-strength of $\approx$25 Sv, indicated by the additional suffix FwOn, see Fig. 7 for further details). Note, relative standard deviation (RSD) exceeds the value of 2.5 in three cases: Pa_d/Th_d; Re3d (RSD = 3.20; $r = 0.82$), Re3d_FwOn (RSD = 3.27; $r = 0.84$) and Pa_p/Th_p Re3d_BtBd_FwOn (RSD = 3.05; $r = 0.93$). Markers are thus located outside of, and are not shown on the panel. See Table A2 for details on the experimental set up. (For interpretation of the references to colour in this figure, the reader is referred to the web version of this article.)

Lateral export affects the distribution of Pa. Figs. 4 and 5 (dashed lines and transparent markers with dashed border lines) indicate the effect of an even stronger AMOC on Pa_d, Th_d, Pa_d/Th_d and Pa_p/Th_p for parameter sets Re3d_Bt_FWOn, Re3d_BtBd_FWOn (Table A2). We find improved agreement between simulated and observed Pa_d and Th_d (Figs. 4a, b, 5). It becomes clear that stronger overturning affects Pa_d and Th_d in a way similar to boundary scavenging and bottom scavenging. Thus, in Re3d_BtBd_FwOn and compared to Re3d_BtBd a smaller magnitude of additional sinks is required to obtain similar agreement with observations for Pa_d and Th_d.

Following the 2d-approach of Marchal et al. (2000), we find that the overall sink for Pa and Th is more pronounced due to larger adsorption constants at depth and therefore that less additional scavenging at ocean boundaries and/or at the seafloor is required to obtain reasonable agreement with observations (Fig. 4).

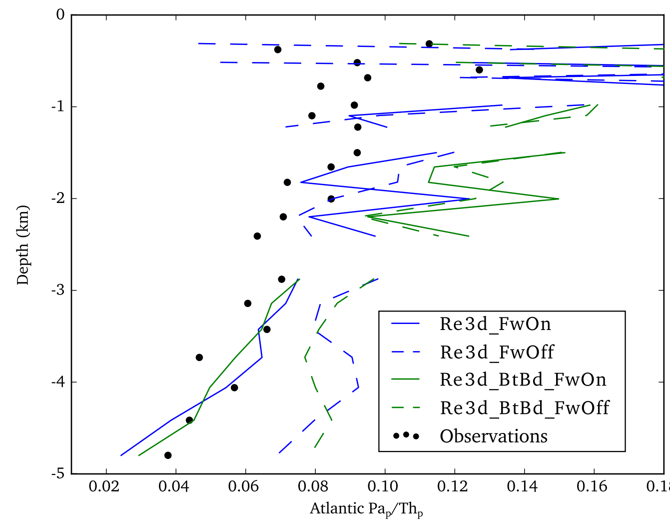

Fig. 6. Atlantic (from 34°S–71°N, excluding the Southern Ocean) profile of simulated Pa_p/Th_p for AMOC on- (as indicated by the additional suffix FwOn, solid lines) and off-states (indicated by the suffix FwOff, dashed lines). Simulated values are taken from grid cells where observations are available. If more than one observation is available at one depth, the weighted mean is shown. Gaps in the profiles are due to missing observations at certain depths. AMOC is periodically turned off and on by applying positive and negative freshwater perturbations (±0.3 Sv, similar to Rempfer et al. (2012)) to the North Atlantic (45 to 70°N). Values are averaged over 1 kyr, as indicated by grey bars in Fig. 7. Further details on the experimental set up are given in Table A2. Basin mean of available observations from sediment surfaces are indicated by black dots (see Table A3, for references).

4.1. *Comparison with previous studies and further implications*

Simulated Pa_d and Th_d exceeded observed values in previous studies by Siddall et al. (2005) and Dutay et al. (2009) as well. In contrast, Pa_d and Th_d were simulated in agreement with observations by Marchal et al. (2000).

Apart from the magnitude of the additional boundary scavenging as mentioned above, one explanation for the reasonable agreement in the study of Marchal et al. (2000) is the strong AMOC ($\approx$24 Sv), compared to studies of Siddall et al. (2005) ($\approx$14 Sv) and Dutay et al. (2009) ($\approx$17.5 Sv). Another explanation is the larger affinity (larger σ_0) of ^{231}Pa and ^{230}Th to particle surfaces, in particular to opal (Table A1). We tested the effect of larger σ_0 (Fig. 1). On the one hand, we find better overall agreement between simulated and observed Pa_d and Th_d. On the other hand, agreement is less pronounced for Pa_p/Th_p (in particular in the Equatorial Pacific, the South Atlantic and the Southern Ocean, not shown). One reason that Pa_p/Th_p e.g., in the Equatorial Pacific or the South Atlantic is not affected by the more pronounced particle affinity in the study of Marchal et al. (2000) is that export production of opal was represented in a simplified manner.

No opal export outside the Southern Ocean was taken into account by Marchal et al. (2000) and no opal export outside the Southern Ocean, the North Pacific and the Arctic was considered by Siddall et al. (2005, their Fig. 1). In contrast, in our study, where particle export production is calculated from prognostic equations, export production of opal is simulated not only in the Southern Ocean opal belt and the North Pacific, but also in the Equatorial Pacific, the South Atlantic off Africa and in the North Atlantic (Fig. A1). The simulated patterns and globally integrated magnitudes of export production are consistent with estimates presented by Sarmiento and Gruber (2006).

5. Pa_p/Th_p during AMOC on/off-states

In this section we examine differences between spatially and temporally averaged profiles of Pa_p/Th_p during AMOC-on-

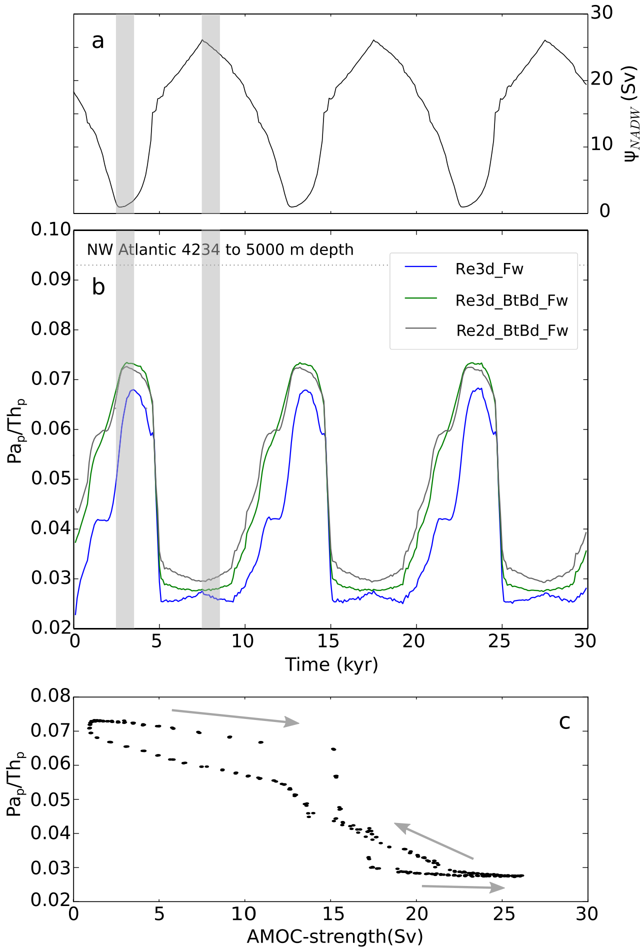

Fig. 7. (a) AMOC-strength and (b) regionally averaged Pa_p/Th_p from the NW Atlantic region (4234 to 5000 m depth) (b) for experiments in which AMOC is periodically turned off and on by applying positive and negative freshwater perturbations (±0.3 Sv, similar to Rempfer et al., 2012) to the North Atlantic (45 to 70°N). Grey bars indicate periods of 1 kyr over which averages are calculated for AMOC Off/On states (FwOff and FwOn, left and right grey bar respectively). (c) A cross-plot indicates the relationship between AMOC-strength and Pa_p/Th_p in this region for parameter set Re3d_BtBd_Fw. The direction of cycling is indicated by arrows. Atlantic overturning stream functions for mean On and Off-states are indicated in Fig. A2. Further details on the experimental set up are given in Table A2.

states and AMOC-off-states in the Northwest Atlantic, an important oceanic region for reconstructions of past changes in AMOC strength (e.g., McManus et al., 2004; Ritz et al., 2013; Böhm et al., 2015) (Fig. 6). Time periods for which averages of Pa_p/Th_p and AMOC-strength are calculated span 1 kyr and are indicated by grey bars in Fig. 7. Average AMOC-strength during on-state approximates 24 Sv, average AMOC-strength during off-state is close to 0 Sv (Fig. A2b, c). Although these time slices do not represent a real steady-state, quasi steady-state may be assumed for ^{231}Pa and ^{230}Th due to the long periodicity of the freshwater-forcing and the relatively short mean residence times of ^{231}Pa and ^{230}Th.

During on-states and at depths greater than about 1 km, Pa_p/Th_p linearly decreases from 0.10–0.12 to 0.04–0.06 dependent on the parameter set (indicated by solid lines in Fig. 6). In contrast during off-states the decrease in Pa_p/Th_p with depth is less pronounced (from 0.09–0.10 to 0.07–0.08, indicated by dashed lines in Fig. 6).

A linear decrease in Pa_p/Th_p with depth has been observed at different locations (Walter et al., 2000). At first, this decrease was ascribed to changes in particle composition (Scholten et al., 2008). Subsequent studies however argued that it reflects lateral export of Pa from the Atlantic to the Southern Ocean by NADW (Gherardi et al., 2009; Luo et al., 2010; Lippold et al., 2011, 2012).

Our results indicate that overturning-strength largely affects the depth-evolution of Pa_p/Th_p and thus support the reasoning of Luo et al. (2010) and Lippold et al. (2011). It is important to note however, that Pa_p/Th_p does not simply reach the production ratio in case of halted AMOC (which agrees with Luo et al., 2010). Instead, during AMOC-off-states, Pa_p/Th_p is greater than the production-ratio at depths shallower than about 2–3 km and is smaller at greater depths. This may be due to the fact that circulation is not halted completely, e.g., wind-driven circulation (Fig. A2c) and that lateral transport (diffusion) in particular of Pa into regions of higher export productivity remains effective during a slowdown of the AMOC (Roberts et al., 2014).

6. Pa_p/Th_p in transient perturbation simulations

Similar to Rempfer et al. (2012) we examine the effect of transient changes in AMOC-strength on spatially-averaged Pa_p/Th_p in the Northwest Atlantic for different parameter sets (Re3d, Re3d_BtBd, Re2d_BtBd, Fig. 7). Therefore, we apply periodic freshwater perturbations (±0.3 Sv) of durations of $T_{Fw} = 10$ kyr to the North Atlantic, which results in a periodic collapse and resumption of the AMOC (Fig. 7a). Maximum AMOC-strength, ψ_{AMOC}, varies from about 0–26 Sv. These end-member experiments are highly idealised and thus not directly comparable to past changes in ocean circulation. Instead we aim to examine effects of changes in overturning strength on Pa_p/Th_p and compare these effects to those of the above mentioned processes.

Spatially-averaged deep ocean Pa_p/Th_p in the Northwest Atlantic shows large temporal variations which appear to be closely related to variations in ψ_{AMOC} (Fig. 7b, c). Largest values of Pa_p/Th_p (≈ 0.07) occur during AMOC-off-state, smallest values (≈ 0.03) occur during AMOC-on-state. As discussed above, Pa_p/Th_p exceeds the production ratio of 0.093 during AMOC-off-state at depths above of 2–3 km and reaches values slightly smaller than 0.093 below.

Temporal patterns and absolute changes in Pa_p/Th_p are very similar for individual parameter sets despite substantial differences in mean residence times of ^{231}Pa and ^{230}Th (Fig. 7b). This indicates that processes such as reversible scavenging, boundary scavenging and bottom scavenging do not substantially disturb the relationship between overturning strength and Pa_p/Th_p at least on the larger spatial and temporal scales considered in these experiments.

Although the relationship between Pa_p/Th_p in the Northwest Atlantic and ψ_{AMOC} is close, it is not 1:1 (Fig. 7c). This may partly be due to the fact that ψ_{AMOC} reflects overturning strength within the 3-dimensional Atlantic basin and cannot be expected to capture spatial heterogeneity in Pa_p/Th_p at any specific site. In addition, we find differences in the relationship between Pa_p/Th_p and ψ_{AMOC} for decreasing and increasing ψ_{AMOC}: The relationship between decreasing AMOC-strength (and increasing Pa_p/Th_p) is about linear. In contrast, Pa_p/Th_p shows a shows a step like decrease from 0.07 to 0.03 (between 15 and 20 Sv, grey arrows indicate the direction of cycling in Fig. 7c) for increasing AMOC-strength.

We spatially extended our analysis of the relationship between Pa_p/Th_p and ψ_{AMOC} for parameter set Re3d_BtBd to GEOTRACES transect GA03. Correlation coefficients indicate a more pronounced relationship at greater depths (Fig. 8a). Similarly, changes in Pa_p/Th_p per unit change in ψ_{AMOC} are larger at greater depths (Fig. 8b). We therefore suggest not to simply use the regression slopes as shown in Fig. 8b for the interpretation of reconstructed changes of Pa_p/Th_p from sediment cores. Instead, spatial patterns in Fig. 8a, b indicate that our model simulates the classical relationship between Pa_p/Th_p and ψ_{AMOC} (negative correlation) pri-

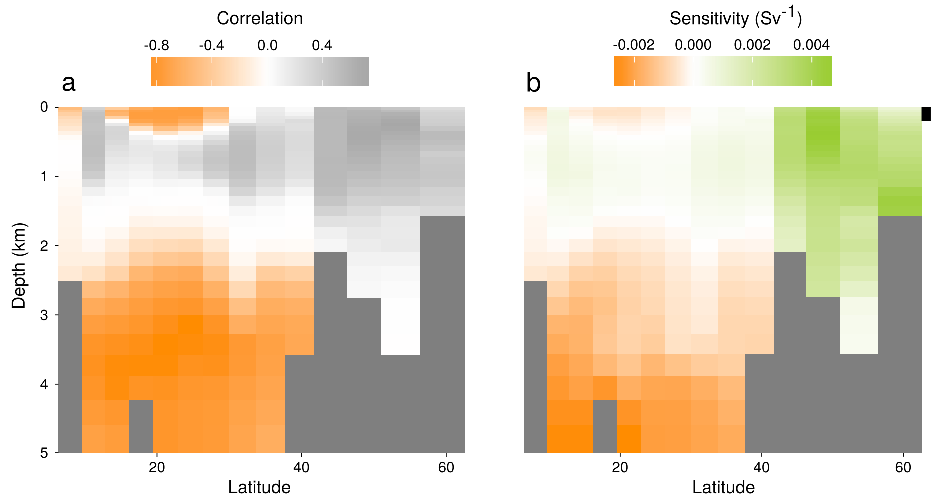

Fig. 8. (a) Correlation coefficients ($r \cdot |r|$) and (b) slope (i.e., overturning sensitivity of Pa_p/Th_p (Sv^{-1})) of linear regression model for the relationship between Pa_p/Th_p and ψ_{AMOC} along GEOTRACES transect GA03 in the North Atlantic (the course of the track is indicated in Fig. A4) for parameter set Re3d_BtBd. Correlation coefficients are derived from non-parametric Kendall rank correlation, linear regression models are based on the non-parametric Theil-Sen approach. Note the asymmetric colour gradient.

marily in the North Atlantic at depths below 2 km. In more northern latitudes and depths above 2 km the correlation is positive, i.e., increasing Pa_p/Th_p ratios indicate increasing ψ_{AMOC}. We stress that this spatially dependent behaviour of the paleoceanographic tracer of AMOC variations should be investigated in more detail using a better resolved ocean-tracer model.

7. Summary, conclusions and outlook

Our major findings are: (i) Given the available observational data sets, no single model can be defined, which yields maximum agreement for each of Pa_d, Pa_p, Th_d, Th_p and Pa_p/Th_p based on the classical concept of reversible scavenging of ^{231}Pa and ^{230}Th by particles in the water column alone.

(ii) Taking into account additional sinks at the seafloor and at ocean margins (simplified representations of bottom and boundary scavenging) yields improved agreement with observations in particular for Atlantic Pa_d, Th_d, Pa_d/Th_d and to a smaller extent for Pa_p/Th_p. This indicates that additional sinks such as nepheloid layers and boundary scavenging are important sinks of ^{231}Pa and ^{230}Th and that lateral export of ^{231}Pa is particularly important for shaping profiles of Pa_d.

(iii) Atlantic profiles of Pa_p/Th_p decrease with depth in all parameter sets during AMOC-on and off-states. The rate of the decrease depends on the parameter set and is reduced during AMOC-off-states but does not approach zero in any parameter set at great depths (below $\approx$ 3000 m). Even during AMOC off-states Pa_p/Th_p does not simply approach the production ratio. Lateral export of ^{231}Pa into regions of high particle flux, such as at continental boundaries, may remove Pa from the open ocean despite halted overturning.

(iv) Marked variations in Pa_p/Th_p are observed at great depths in the Northwest Atlantic in experiments in which ocean circulation is turned on and off in a transient way. This relationship is robust across parameter sets examined in this study and is not much affected by differences in the marine cycle of ^{231}Pa and ^{230}Th, for instance mean residence times.

Although our approach is a step forward compared to previous studies we are aware that it is still based on strong simplifications which do not allow accurate representations of real world processes: only three particle types and one particle size class are considered in the present version of the carbon cycle model; dissolution profiles and settling speed are globally uniform; nepheloid layers and boundary scavenging as well as fractionation of ^{231}Pa and ^{230}Th by different particle types are represented in a simplified manner. These simplifications on the one hand are due to the missing understanding of processes and on the other hand are due to the coarse resolution of our model. Nonetheless, on larger regional scales our results yield meaningful insights. However, a better understanding of the effects of these processes is required for a reasonable simulation of smaller-scale patterns in particular of Pa_d. This will also lead to increased confidence in Pa_p/Th_p-based reconstructions of past changes in AMOC.

Acknowledgements

This work is supported by the Swiss National Science Foundation by grants 200020_147114 and PP00P2_144811 and by the European Commission through the FP7 projects Past4Future (grant No. 243908) and CARBOCHANGE (grant No. 264879). JL was supported by the FP7-PEOPLE-2013-IEF, Marie-Curie proposal 622483, OCEANQUANT and by DFG grant Li1815/4. Constructive reviews of A. Thomas and two anonymous reviewers are gratefully acknowledged. Data which have been used to produce the results of this paper can be obtained from JR.

Appendix A. Supplementary material

Supplementary material related to this article can be found online at http://dx.doi.org/10.1016/j.epsl.2017.03.027.

References

Anderson, R.F., Bacon, M.P., Brewer, P.G., 1983a. Removal of ^{230}Th and ^{231}Pa at ocean margins. Earth Planet. Sci. Lett. 66, 73–90. http://dx.doi.org/10.1016/0012-821X(83)90127-9. http://www.sciencedirect.com/science/article/pii/0012821X83901279.

Anderson, R.F., Bacon, M.P., Brewer, P.G., 1983b. Removal of ^{230}Th and ^{231}Pa from the open ocean. Earth Planet. Sci. Lett. 62 (1), 7–23. http://www.sciencedirect.com/science/article/pii/0012821X83900675.

Bacon, M., Anderson, R., 1982. Distribution of thorium isotopes between dissolved and particulate forms in the deep sea. J. Geophys. Res. 87, 2045–2056. http://dx.doi.org/10.1029/JC087iC03p02045.

Biscaye, P.E., Eittreim, S.L., 1977. Suspended particulate loads and transports in the nepheloid layer of the abyssal Atlantic Ocean. Mar. Geol. 23 (1–2), 155–172. http://www.sciencedirect.com/science/article/pii/0025322777900871.

Böhm, E., Lippold, J., Gutjahr, M., Frank, M., Blaser, P., Antz, B., Fohlmeister, J., Frank, N., Andersen, M.B., Deininger, M., 2015. Strong and deep Atlantic Meridional Overturning Circulation during the last glacial cycle. Nature 517, 73–76. http://dx.doi.org/10.1038/nature14059.

Chase, Z., Anderson, R.F., Fleisher, M.Q., Kubik, P.W., 2002. The influence of particle composition and particle flux on scavenging of Th, Pa and Be in the ocean. Earth Planet. Sci. Lett. 204 (1–2), 215–229. http://dx.doi.org/10.1016/S0012-821X(02)00984-6. http://www.sciencedirect.com/science/article/pii/S0012821X02009846.

Christl, M., Lippold, J., Hofmann, A., Wacker, L., Lahaye, Y., Synal, H.A., 2010. ^{231}Pa/^{230}Th: a proxy for upwelling off the coast of West Africa, Proceedings of the Eleventh International Conference on Accelerator Mass Spectrometry. Nucl. Instrum. Methods Phys. Res., Sect. B, Beam Interact. Mater. Atoms 268 (7–8), 1159–1162. http://dx.doi.org/10.1016/j.nimb.2009.10.123. http://www.sciencedirect.com/science/article/pii/S0168583X09011720.

Deng, F., Thomas, A.L., Rijkenberg, M.J., Henderson, G.M., 2014. Controls on seawater ^{231}Pa, ^{230}Th and ^{232}Th concentrations along the flow paths of deep waters in the Southwest Atlantic. Earth Planet. Sci. Lett. 390, 93–102. http://www.sciencedirect.com/science/article/pii/S0012821X1300753X.

Doney, S.C., Lindsay, K., Fung, I., John, J., 2006. Natural variability in a stable 1000 year global coupled climate-carbon cycle simulation. J. Climate 19, 3033–3054.

Dutay, J.C., Lacan, F., Roy-Barman, M., Bopp, L., 2009. Influence of particle size and type on ^{231}Pa and ^{230}Th simulation with a global coupled biogeochemical-ocean general circulation model: a first approach. Geochem. Geophys. Geosyst. 10 (1), Q01011. http://dx.doi.org/10.1029/2008GC002291.

Gherardi, J.M., Labeyrie, L., Nave, S., Francois, R., McManus, J.F., Cortijo, E., 2009. Glacial-interglacial circulation changes inferred from ^{231}Pa/^{230}Th sedimentary record in the North Atlantic region. Paleoceanography, 24. http://dx.doi.org/10.1029/2008PA001696.

Hayes, C.T., Anderson, R.F., Fleisher, M.Q., Huang, K.F., Robinson, L.F., Lu, Y., Cheng, H., Edwards, R.L., Moran, S.B., 2015a. ^{230}Th and ^{231}Pa on {GEOTRACES} GA03, the U.S. {GEOTRACES} North Atlantic transect, and implications for modern and paleoceanographic chemical fluxes. Deep-Sea Res., Part 2, Top. Stud. Oceanogr. 116, 29–41. http://dx.doi.org/10.1016/j.dsr2.2014.07.007. http://www.sciencedirect.com/science/article/pii/S0967064514001799. {GEOTRACES} GA-03. The U.S. {GEOTRACES} North Atlantic Transect.

Hayes, C.T., Anderson, R.F., Fleisher, M.Q., Lam, P.J., Ohnemus, D.C., Kuo-Fang, H., Robinson, L.F., Lu, Y., Cheng, H., Edwards, R.L., Moran, S.B., 2015b. Intensity of Th and Pa scavenging partitioned by particle chemistry in the North Atlantic Ocean. Mar. Chem. http://dx.doi.org/10.1016/j.marchem.2015.01.006. http://www.sciencedirect.com/science/article/pii/S0304420315000183.

Henderson, G., Heinze, C., Anderson, R., Winguth, A., 1999. Global distribution of the Th-230 flux to ocean sediments constrained by GCM modelling. Deep-Sea Res., Part 1, Oceanogr. Res. Pap. 46 (11), 1861–1893.

Kretschmer, S., Geibert, W., van der Loeff, M.M.R., Schnabel, C., Xu, S., Mollenhauer, G., 2011. Fractionation of ^{230}Th, ^{231}Pa, and ^{10}Be induced by particle size and composition within an opal-rich sediment of the Atlantic Southern Ocean. Geochim. Cosmochim. Acta 75 (22), 6971–6987. http://dx.doi.org/10.1016/j.gca.2011.09.012. http://www.sciencedirect.com/science/article/pii/S0016703711005333.

Lam, P.J., Ohnemus, D.C., Auro, M.E., 2015. Size-fractionated major particle composition and concentrations from the {US} {GEOTRACES} North Atlantic zonal transect. Deep-Sea Res., Part 2, Top. Stud. Oceanogr. 116, 303–320. http://dx.doi.org/10.1016/j.dsr2.2014.11.020. http://www.sciencedirect.com/science/article/pii/S0967064514003270. {GEOTRACES} GA-03. The U.S. {GEOTRACES} North Atlantic Transect.

Lippold, J., Gherardi, J.M., Luo, Y., 2011. Testing the ^{231}Pa/^{230}Th paleocirculation proxy: a data versus 2D model comparison. Geophys. Res. Lett. 38 (20), L20603. http://dx.doi.org/10.1029/2011GL049282.

Lippold, J., Mulitza, S., Mollenhauer, G., Weyer, S., Heslop, D., Christl, M., 2012. Boundary scavenging at the East Atlantic margin does not negate use of ^{231}Pa/^{230}Th to trace Atlantic overturning. Earth Planet. Sci. Lett. 333–334, 317–331. http://www.sciencedirect.com/science/article/pii/S0012821X12001720.

Luo, Y., Francois, R., Allen, S.E., 2010. Sediment ^{231}Pa/^{230}Th as a recorder of the rate of the Atlantic meridional overturning circulation: insights from a 2-D model. Ocean Sci. 6 (1), 381–400. http://dx.doi.org/10.5194/os-6-381-2010. http://www.ocean-sci.net/6/381/2010/.

Marchal, O., Francois, R., Stocker, T.F., Joos, F., 2000. Ocean thermohaline circulation and sedimentary ^{231}Pa/^{230}Th ratio. Paleoceanography 15, 625–641.

Martin, J., 1990. Glacial–interglacial CO_2 change: the iron hypothesis. Paleoceanography 5, 1–13. http://www.agu.org/journals/pa/v005/i001/PA005i001p00001/.

McManus, J.F., Francois, R., Gherardi, J.M., Keigwin, L.D., Brown-Leger, S., 2004. Collapse and rapid resumption of Atlantic meridional circulation linked to deglacial climate changes. Nature 428. http://dx.doi.org/10.1038/nature02494.

Moran, S., Shen, C.C., Edmonds, H., Weinstein, S., Smith, J., Edwards, R., 2002. Dissolved and particulate ^{231}Pa and ^{230}Th in the Atlantic Ocean: constraints on intermediate/deep water age, boundary scavenging, and ^{231}Pa/^{230}Th fractionation. Earth Planet. Sci. Lett. 203 (3–4), 999–1014. http://www.sciencedirect.com/science/article/pii/S0012821X02009287.

Müller, S.A., Joos, F., Edwards, N.R., Stocker, T.F., 2006. Water mass distribution and ventilation time scales in a cost-efficient, three-dimensional ocean model. J. Climate 19, 5479–5499.

Nozaki, Y., Nakanishi, T., 1985. ^{231}Pa and ^{230}Th profiles in the open ocean water column. Deep-Sea Res., A, Oceanogr. Res. Pap. 32 (10), 1209–1220. http://www.sciencedirect.com/science/article/pii/0198014985900044.

Oka, A., Hasumi, H., Obata, H., Gamo, T., Yamanaka, Y., 2009. Study on vertical profiles of rare earth elements by using an ocean general circulation model. Glob. Biogeochem. Cycles 23, GB4025. http://dx.doi.org/10.1029/2008GB003353.

Okubo, A., Obata, H., Gamo, T., Yamada, M., 2012. ^{230}Th and ^{232}Th distributions in mid-latitudes of the North Pacific Ocean: effect of bottom scavenging. Earth Planet. Sci. Lett. 339–340, 139–150. http://www.sciencedirect.com/science/article/pii/S0012821X12002245.

Parekh, P., Joos, F., Müller, S.A., 2008. A modeling assessment of the interplay between aeolian iron fluxes and iron-binding ligands in controlling carbon dioxide fluctuations during Antarctic warm events. Paleoceanography 23, PA4202. http://dx.doi.org/10.1029/2007PA001531.

Plattner, G.K., Joos, F., Stocker, T.F., Marchal, O., 2001. Feedback mechanisms and sensitivities of ocean carbon uptake under global warming. Tellus B 53 (5), 564–592. http://dx.doi.org/10.1034/j.1600-0889.2001.530504.x.

Rempfer, J., Stocker, T.F., Joos, F., Dutay, J.C., 2012. On the relationship between Nd isotopic composition and ocean overturning circulation in idealized freshwater discharge events. Paleoceanography 27 (3), PA3211. http://dx.doi.org/10.1029/2012PA002312.

Rempfer, J., Stocker, T.F., Joos, F., Dutay, J.C., Siddall, M., 2011. Modelling Nd-isotopes with a coarse resolution ocean circulation model: sensitivities to model parameters and source/sink distributions. Geochim. Cosmochim. Acta 75 (20), 5927–5950. http://dx.doi.org/10.1016/j.gca.2011.07.044. http://www.sciencedirect.com/science/article/pii/S001670371100442X.

Ritz, S.P., Stocker, T.F., Grimalt, J.O., Menviel, L., Timmermann, A., 2013. Estimated strength of the Atlantic overturning circulation during the last deglaciation. Nat. Geosci. 6, 208–212. http://dx.doi.org/10.1038/ngeo1723. http://www.nature.com/ngeo/journal/v6/n3/abs/ngeo1723.html#supplementary-information.

Ritz, S.P., Stocker, T.F., Joos, F., 2011. A coupled dynamical ocean energy balance atmosphere model for paleoclimate studies. J. Climate 24 (2), 349–375. http://dx.doi.org/10.1175/2010JCLI3351.1. http://journals.ametsoc.org/doi/abs/10.1175/2010JCLI3351.1. http://journals.ametsoc.org/doi/pdf/10.1175/2010JCLI3351.1.

Roberts, N.L., McManus, J.F., Piotrowski, A.M., McCave, I.N., 2014. Advection and scavenging controls of Pa/Th in the northern NE Atlantic. Paleoceanography 29 (6), 2014PA002633. http://dx.doi.org/10.1002/2014PA002633.

Roy-Barman, M., 2009. Modelling the effect of boundary scavenging on thorium and protactinium profiles in the ocean. Biogeosciences 6 (12), 3091–3107. http://dx.doi.org/10.5194/bg-6-3091-2009. http://www.biogeosciences.net/6/3091/2009/.

Sarmiento, J.L., Gruber, N., 2006. Ocean Biogeochemical Dynamics. Princeton University Press.

Schmittner, A., 2005. Decline of the marine ecosystem caused by a reduction in the Atlantic overturning circulation. Nature 434, 628–633. http://dx.doi.org/10.1038/nature03476.

Scholten, J., Fietzke, J., Mangini, A., Stoffers, P., Rixen, T., Gaye-Haake, B., Blanz, T., Ramaswamy, V., Sirocko, F., Schulz, H., Ittekkot, V., 2005. Radionuclide fluxes in the Arabian Sea: the role of particle composition. Earth Planet. Sci. Lett. 230 (3–4), 319–337. http://www.sciencedirect.com/science/article/pii/S0012821X04006727.

Scholten, J.C., Fietzke, J., Mangini, A., Garbe-Schönberg, C.D., Eisenhauer, A., Schneider, R., Stoffers, P., 2008. Advection and scavenging: effects on ^{230}Th and ^{231}Pa distribution off Southwest Africa. Earth Planet. Sci. Lett. 271 (1–4), 159–169. http://www.sciencedirect.com/science/article/pii/S0012821X08002288.

Siddall, M., Henderson, G.M., Edwards, N.R., Frank, M., Müller, S.A., Stocker, T.F., Joos, F., 2005. ^{231}Pa/^{230}Th fractionation by ocean transport, biogenic particle flux and particle type. Earth Planet. Sci. Lett. 237 (1–2), 135–155. http://dx.doi.org/10.1016/j.epsl.2005.05.031. http://www.sciencedirect.com/science/article/B6V61-4GNKRXK-2/2/1efb044db6cdae3b869b3f2d5d9c6668.

Siddall, M., Stocker, T.F., Henderson, G.M., Joos, F., Frank, M., Edwards, N.R., Ritz, S.P., Müller, S.A., 2007. Modeling the relationship between ^{231}Pa/^{230}Th distribution in North Atlantic sediment and Atlantic meridional overturning circulation. Paleoceanography 22, PA2214.

Srokosz, M.A., Bryden, H.L., 2015. Observing the Atlantic meridional overturning circulation yields a decade of inevitable surprises. Science 348, 6241. http://dx.doi.org/10.1126/science.1255575. http://www.sciencemag.org/content/348/6241/1255575.abstract. http://www.sciencemag.org/content/348/6241/1255575.full.pdf.

Talley, L.D., Reid, J.L., Robbins, P.E., 2003. Data-based meridional overturning streamfunctions for the global ocean. J. Climate 16 (19), 3213. http://dx.doi.org/10.1175/1520-0442(2003)016<3213:DMOSFT>2.0.CO;2.

Taylor, K.E., 2001. Summarizing multiple aspects of model performance in a single diagram. J. Geophys. Res. 106 (D7), 7183–7192. http://dx.doi.org/10.1029/2000JD900719.

Thomas, A.L., Henderson, G.M., Robinson, L.F., 2006. Interpretation of the ^{231}Pa/^{230}Th paleocirculation proxy: new water-column measurements from the southwest Indian Ocean. Earth Planet. Sci. Lett. 241 (3–4), 493–504. http://dx.doi.org/10.1016/j.epsl.2005.11.031. http://www.sciencedirect.com/science/article/B6V61-4HYD9NM-1/2/c4b9600338c10f6045a64cbaaeb4976b.

Tschumi, T., Joos, F., Parekh, P., 2008. How important are Southern Hemisphere wind changes for low glacial carbon dioxide? A model study. Paleoceanography 23, PA4208. http://dx.doi.org/10.1029/2008PA001592.

Walter, H., van der Loeff, Rutgers M., Hoeltzen, H., 1997. Enhanced scavenging of ^{231}Pa relative to ^{230}Th in the South Atlantic south of the Polar Front: implications for the use of the ^{231}Pa/^{230}Th ratio as a paleoproductivity proxy. Earth Planet. Sci. Lett. 149 (1–4), 85–100. http://www.sciencedirect.com/science/article/pii/S0012821X9700068X.

Walter, H., van der Loeff, M.R., Hltzen, H., Bathmann, U., 2000. Reduced scavenging of ^{230}Th in the Weddell Sea: implications for paleoceanographic reconstructions in the South Atlantic. Deep-Sea Res., Part 1, Oceanogr. Res. Pap. 47 (7), 1369–1387. http://dx.doi.org/10.1016/S0967-0637(99)00094-1. http://www.sciencedirect.com/science/article/pii/S0967063799000941.

Yu, E.F., Francois, R., Bacon, M.P., 1996. Similar rates of modern and last-glacial ocean thermohaline circulation inferred from radiochemical data. Nature 379 (6567), 689–694. http://dx.doi.org/10.1038/379689a0.